Response of a Polarimetric Antenna to Ionospherically Propagated Signals

Lenard Pederick, Trevor Harris, Andrew MacKinnon, and Iain Reid, *Senior Member, IEEE*

***Abstract*— The Earth's magnetic field causes the ionosphere to be birefringent at radio frequencies, which means that any system using ionospherically propagated radio waves, such as long-distance broadcasting, high-frequency (HF) skywave communications, over-the-horizon radar, and oblique incidence sounders (OIS) will receive pairs of waves with different polarizations. In this article, we develop a model for the polarization of ionospherically propagated radio waves; the polarization is dependent only upon the strength and direction of the magnetic field at the location where the radio wave exits the ionosphere. This leads to the hemisphere of possible incoming directions of arrival to any particular receiver being divided into three distinct regions. We then use this model to predict the response of a polarimetric antenna to a transmitted OIS signal and validate the model against real ionograms, including cases where all three polarization regions can be clearly observed.**

***Index Terms*— Ionosphere, polarimetry, radiowave propagation, skywave propagation.**

I. Introduction

DUE to the Earth's magnetic field, the ionosphere is birefringent at radio frequencies—there are two canonical propagation modes corresponding to the polarization of the radio waves, termed the ordinary (O) and extraordinary (X) modes. The actual polarizations of these two modes will vary depending on the angle between the magnetic field and the wave's direction of propagation, as well as the wave frequency and the strength of the magnetic field [1]. This birefringence means that any system using ionospherically propagated radio waves—such as long-distance broadcasting, high-frequency (HF) skywave communications, and over-the-horizon radar—will receive pairs of waves with different polarizations. This can cause many effects on these systems, including loss of sensitivity due to polarization mismatch, multipath effects, and polarization fading. A good understanding of the polarization of the received radio waves is necessary for predicting the effectiveness of such systems.

Vertical-incidence sounders (VISs) and oblique-incidence sounders (OISs) use the time delay of ionospherically propagated HF radio waves to measure the state of the ionosphere. The separation of the two propagation modes on a VIS using a polarimetric receive antenna is a well-established technique [2]–[5].

In previous work [6], a method for separating the polarization modes for OIS was developed; however, this method assumes that both modes are circularly polarized. In this article, we will develop a model for the polarization of incoming OIS signals and demonstrate its validity using OIS soundings received by a polarimetric receive antenna, which specifically show some of the unique phenomena predicted by the model.

Manuscript received October 25, 2020; revised March 24, 2021; accepted April 13, 2021. Date of publication June 21, 2021; date of current version October 28, 2021. *(Corresponding author: Lenard Pederick.)*

Lenard Pederick and Trevor Harris are with the Defence Science and Technology Group, Edinburgh, SA 5111, Australia, and also with the School of Physical Sciences, University of Adelaide, Adelaide, SA 5005, Australia (e-mail: lenard.pederick@dst.defence.gov.au).

Andrew MacKinnon and Iain Reid are with the School of Physical Sciences, University of Adelaide, Adelaide, SA 5005, Australia.

Color versions of one or more figures in this article are available at https://doi.org/10.1109/TAP.2021.3088283.

Digital Object Identifier 10.1109/TAP.2021.3088283

TABLE I

LOCATIONS OF OIS TRANSMITTERS, SHOWING DISTANCE AND BEARING FROM THE RECEIVER AT KOWANDI

Site name	Code	Latitude	Longitude	Distance (km)	Bearing
Kalkarindji	KAL	17.44°S	130.83°E	547	182.7°
Scherger	SCH	12.65°S	142.09°E	1198	89.4°

II. Polarimetric Receive Antenna

In this study, we used a polarimetric receive antenna consisting of a pair of 1.5 m × 1.5 m galvanized steel magnetic cross loops, as shown in Fig. 1. The two loops are each fed by a 4:1 passive transformer balun, at the center of the base of the loops, and are electrically isolated from the central mast using nylon bolts and sleeves, as well as isolated from each other. This is the same antenna design used in the PRIME ionospheric sounder systems [7].

For this study, the receiver was located at Kowandi, 12.54° S, 131.06° E (magnetic latitude of 22.47° S). At this location, the magnetic field has a declination of 2.5° and an inclination of −39.6°. The planes of the two loops were oriented at true bearings of −65° and 25°.

The receiver was used to receive OIS signals transmitted from two locations, as shown in Table I and Fig. 2.

III. Wave Polarization

While a radio wave is propagating through the ionosphere, its polarization will be one of the two characteristic polarizations supported by the ionosphere; these two polarizations will have different indices of refraction, thus any radio wave which has a polarization different from either of these will be split into two waves (an O and an X wave) each with one of the two characteristic polarization.

Fig. 1. Polarimetric receive antenna of the same type as used in this study.

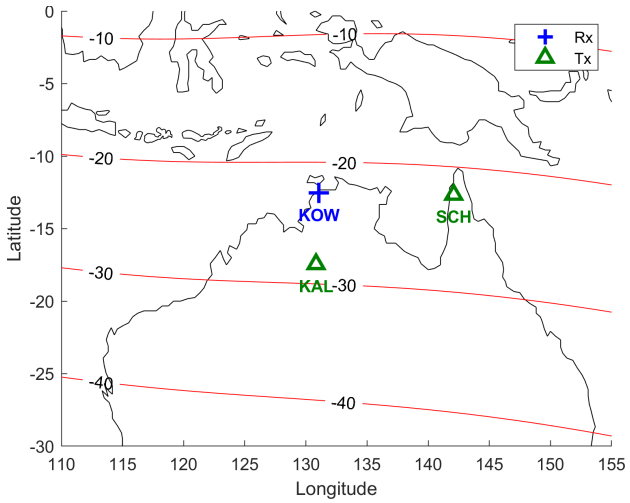

Fig. 2. Map showing the locations of the receiver and the two transmitters used in this article, with lines of magnetic latitude also shown.

If we consider a plane electromagnetic wave of angular frequency ω traveling through an anisotropic, collisionless plasma, in the x-direction of an orthogonal system of axes, in which the external magnetic field lies in the xy plane and makes an angle Θ with the direction of propagation, it can be shown that the wave polarization ρ is given by Budden [1]

$$\rho = \frac{E_z}{E_y} = -\frac{H_y}{H_z} \tag{1}$$

$$\rho^2 - i\rho\frac{Y\sin^2\Theta}{(1-X)\cos\Theta} + 1 = 0 \tag{2}$$

$$\Rightarrow \rho = \frac{\frac{1}{2}iY\sin^2\Theta \pm i\sqrt{\frac{1}{4}Y^2\sin^2\Theta + \cos^2\Theta(1-X)^2}}{(1-X)\cos\Theta} \tag{3}$$

where

$$X = \frac{Ne^2}{\varepsilon_0 m_e\omega^2} = \frac{\omega_N^2}{\omega^2} \tag{4}$$

$$Y = \frac{eB}{m_e\omega} = \frac{\omega_H}{\omega} \tag{5}$$

N is the electron number density, e and m_e are the charge and mass of the electron, ω_N is the plasma frequency, B is the magnitude of the imposed magnetic field, and ω_H is the electron gyrofrequency.

Equation (3) implies that there are two characteristic waves that can propagate in this particular medium; the O and X modes, with corresponding wave polarizations ρ_O and ρ_X. $\rho_O\rho_X = 1$, which implies that (due to the definition of ρ) the sense of rotation of the X mode is opposite to that of the O mode (i.e., if one mode has left-handed rotation, the other will have right-handed rotation), and that their major axes are perpendicular. Equation (3) also implies that both ρ_O and ρ_X are purely imaginary; thus, the axis ratio A (ratio between the major and minor axes) and the eccentricity e are given by

$$A = \frac{1}{\|\rho_O\|} = \|\rho_X\| \tag{6}$$

$$e = \sqrt{1 - \|\rho_O\|^2} = \sqrt{1 - \frac{1}{\|\rho_X\|^2}}. \tag{7}$$

Both modes will have the same axis ratio and eccentricity. Note that this is only true for a collisionless plasma; if the effects of collisions are included the two polarizations will not have perpendicular axes [1]. For typical conditions in the Earth's ionosphere, this effect is mostly encountered at the apex of the wave's propagation path, the peak of the E region and in the D region [8]. The effect of collisions on the wave's polarization once it reaches the ground should be negligible: it will generally be set at the base of the E region, as the D region does not refract HF waves significantly and thus will not affect their polarization.

Once the wave leaves the ionosphere, the index of refraction is no longer dependent on its polarization, thus a wave with any polarization can propagate without its polarization changing. We will assume that the polarization received at an antenna at ground level is unchanged from where it left the ionosphere. If the wave's direction of arrival is known, this location can be found by tracing a straight line backwards from the receiver in the modeled direction of arrival, until it reaches the height of the base of the ionosphere. From Fig. 3, it can be shown that the distance along the ground to the point directly below where the wave left the ionosphere, r_{exit}, is given by

$$r_{\text{exit}} = R_E\gamma = R_E\left(\arccos\frac{R_E\cos\theta}{R_E+h} - \theta\right) \tag{8}$$

where R_E is the radius of the earth, θ is the elevation, γ is the angle subtended at the center of the earth by the ray path from the receiver to the base of the ionosphere, and h is the height of the base of the ionosphere.

We will define the base of the ionosphere to be the height below which there is no significant retardation of the radio wave, and thus no significant change in its polarization.

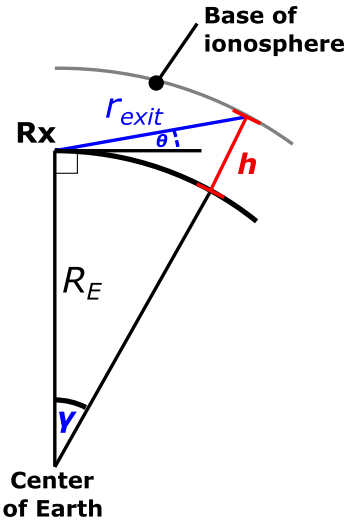

Fig. 3. Geometry used for calculating the location where a given wave left the ionosphere, knowing its direction of arrival and the height h of the base of the ionosphere.

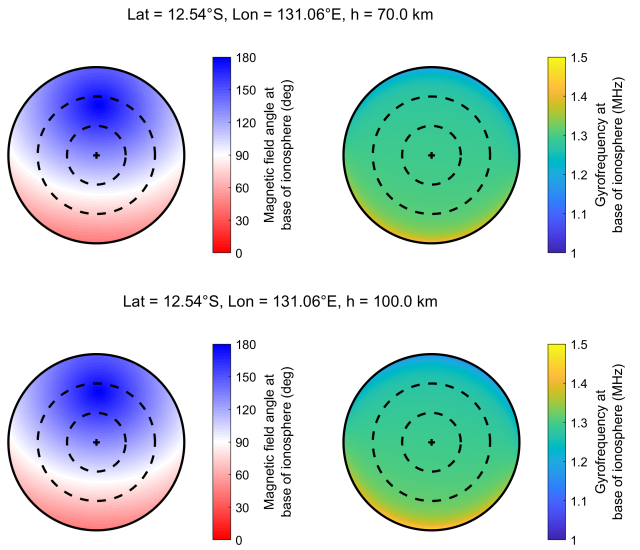

Fig. 4. Magnetic field at the location that a radio wave would exit the ionosphere, calculated for Kowandi, using ionosphere base heights of 70 km (top) and 100 km (bottom). Left panels show Θ, the angle between the wave and the magnetic field; right panels show the electron gyrofrequency. See text for a description of the all-sky projection used here.

This occurs where the electron density approaches zero, thus $X \rightarrow 0$ and from (3)

$$\rho = \frac{\frac{1}{2} i Y \sin^2\Theta \pm i\sqrt{\frac{1}{4}Y^2\sin^4\Theta + \cos^2\Theta}}{\cos\Theta}. \tag{9}$$

This simple derivation ignores that as $X \rightarrow 0$, the indices of refraction of the two polarizations $\eta_O, \eta_X \rightarrow 1$ and the two modes can couple into each other. A more rigorous derivation of this limiting polarization can be found in [9] or [10].

Note that this polarization is dependent only upon the strength and direction of the magnetic field at the location where the radio wave exits the ionosphere. This can be derived from a model of the Earth's magnetic field; we used the International Geomagnetic Reference Field (IGRF-12) [11].

Due to the spatial scale of the Earth's magnetic field, the results obtained via this method are not especially sensitive to the exact height of the base of the ionosphere, as seen in Fig. 4, which shows results calculated using two different heights (70 km for the top row and 100 km for the bottom row).

Note that in this figure, as well as in the following figures, a hemispheric all-sky map is shown using an azimuthal equidistant projection centered on the zenith (shown by a + symbol). Distance from the center is proportional to the zenith angle; the horizon is at the outer edge, and the two dashed circles show 30° and 60° elevation. North is upward and East is to the right. The white lines shown on the two plots on the left side of Fig. 4, where the angle between the wave and the magnetic field is 90°, are shown as a curve in this projection but actually describe the intersection of a flat plane with the hemisphere.

Results from (9) using this magnetic field model are shown in Fig. 5. The left panels show the axis ratio of the O mode and the right panels show the axis ratio of the X mode. Note that the hemisphere of possible incoming directions of arrival can be divided into three regions; near the horizon to the south, where $0° < \Theta < 90°$, the O mode is right elliptically polarized and the X mode is left elliptically polarized. Where $\Theta \approx 90°$, both modes are linearly polarized. In the zenithal and northern directions, where $90° < \Theta < 180°$, the O mode is left elliptically polarized and the X mode is right elliptically polarized.

The effect of the wave's frequency on the polarization can be seen by comparing the two rows; the top row shows the results for 3 MHz and the bottom row shows the results for 10 MHz. Both rows show a similar behavior; in particular, the linearly polarized region is in the same location at all frequencies, and the sense of rotation of the modes is also the same for all frequencies. The main difference is that the higher frequencies are more circular whereas the lower frequencies are more elliptical.

The position of the three regions will depend upon the magnetic field at the receiver's location. For the receiver shown in Fig. 5, south of the magnetic equator, the region of linear polarization is to the south. For a receiver at the magnetic equator, the region of linear polarization will pass through the zenith; for a receiver north of the magnetic equator, it will be to the north.

Note that the magnetic field model used here (IGRF-12) has a limited spatial resolution, with the magnetic field's spherical harmonics specified up to 13th order [11]. Using a magnetic field model with higher spatial resolution may give different results, particularly in the region where $\Theta \approx 90°$. Alternatively, in some situations, it may be useful to simplify the magnetic field model further and approximate it with a locally uniform field.

IV. Direction of Arrival

If we assume a spherically symmetric ionosphere and ignore tilts and gradients, i.e., a spherical mirror model (SMM),

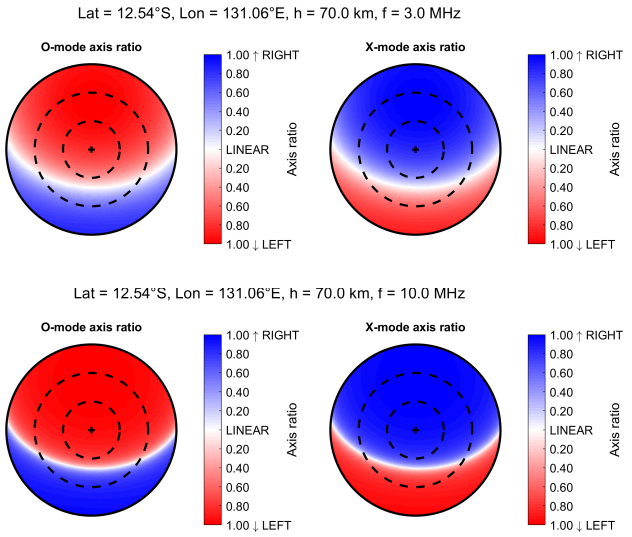

Fig. 5. Polarization of incoming waves, using (9). Top row is results for 3 MHz, bottom row for 10 MHz. Left panels show axis ratio of the O mode, right panels show the X mode.

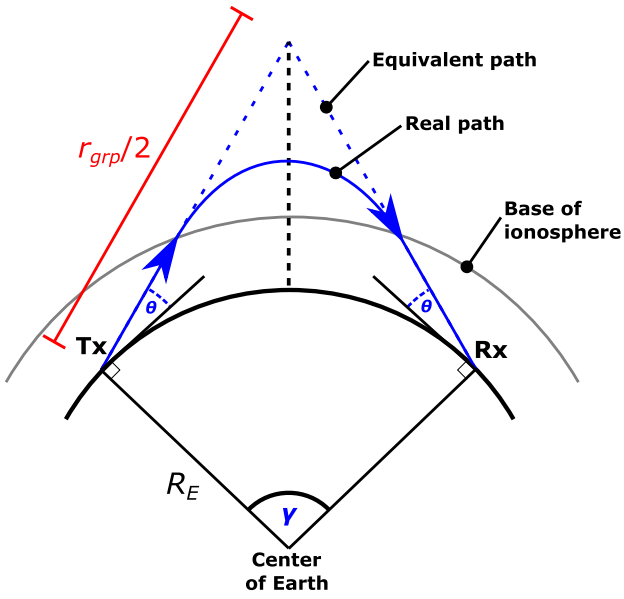

Fig. 6. Geometry used for calculating the elevation angle of an OIS signal via the Breit–Tuve theorem and Martyn's equivalent path theorem.

a relationship between a signal's group delay and its elevation of arrival can be derived. By applying the Breit–Tuve theorem and Martyn's equivalent path theorem [6], [12], [13], we can show that

$$\theta = \arccos\left(\frac{2R_E \sin\frac{\gamma}{2}}{r_{\text{grp}}}\right) - \frac{\gamma}{2} \tag{10}$$

where θ is the elevation angle at the receiver, R_E is the radius of the earth, and $\gamma = (r_{\text{gnd}}/R_E)$ is the angle subtended at the center of the Earth by the sector with the transmitter and receiver as its endpoints, r_{gnd} is the ground range between the transmitter and receiver, and r_{grp} is the group range. The geometry is shown in Fig. 6.

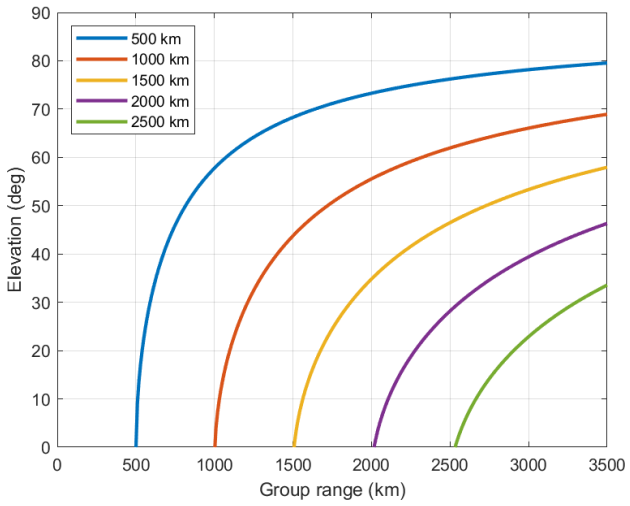

Fig. 7. Elevation versus group range for paths of various ground ranges (shown in legend), from (10).

Fig. 7 shows how θ varies with group range in this model for OIS paths across different ground ranges, assuming an earth radius $R_E = 6376$ km.

In the absence of tilts and gradients, the signal's azimuth should be that of the great circle path between the transmitter and the receiver; unlike elevation, this should not vary as a function of group range.

This SMM will be inaccurate if there are significant tilts or gradients in the ionosphere. There are several known situations where this may occur.

1) Periodic and quasi-periodic traveling ionospheric disturbances (TIDs) will cause various horizontal gradients to appear in the ionosphere, thus causing the direction of arrival to deviate from the SMM [14], [15].
2) At dawn and dusk, the passage of the solar terminator causes large gradients in the ionosphere, and thus deviations in the direction of arrival [16].
3) At longer ground ranges, variations in the ionosphere will be more pronounced and the SMM's core assumption of a spherically symmetric ionosphere will be less accurate.
4) Paths crossing the equatorial anomaly, which causes large and persistent horizontal gradients [17]–[19] as well as disturbances which can cause off-great-circle path reflections [20], [21], will not be modeled accurately by a SMM.
5) Geomagnetic storms can cause disturbances that result in radio wave propagation paths that deviate significantly from those predicted by the SMM [22].

V. Antenna System Response

Knowing the polarization and direction of the incoming wave, we can then determine what the two antenna elements should observe. This requires a conversion from the coordinate system used in Section III, which was defined relative to the wave's propagation and the Earth's magnetic field, to a north-east-up coordinate system in which the antenna is fixed.

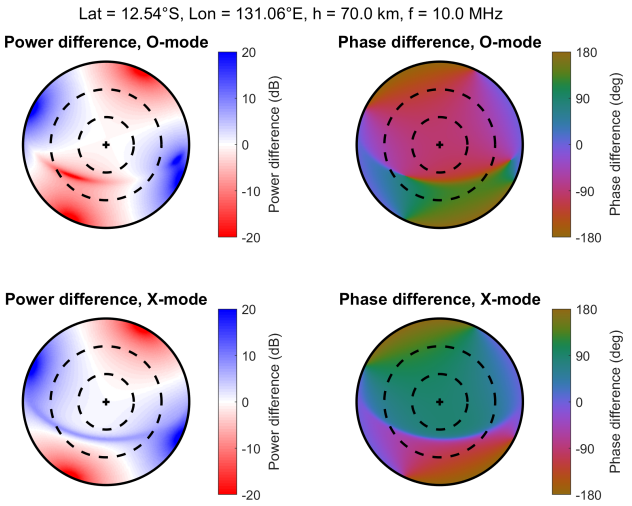

Fig. 8. Predicted response of the polarimetric antenna to incoming ionospherically propagated waves, as modeled in Fig. 5.

The wave's direction of propagation is given by $\hat{\mathbf{x}}$

$$\hat{\mathbf{x}} = \begin{bmatrix} \cos\phi\cos\theta \\ \sin\phi\cos\theta \\ \sin\theta \end{bmatrix} \tag{11}$$

where $\theta \in [0, (\pi/2)]$ is the elevation and $\phi \in [-\pi, +\pi)$ is the azimuth angle.

We can then determine the unit vectors $\hat{\mathbf{y}}$ and $\hat{\mathbf{z}}$

$$\mathbf{y} = \hat{\mathbf{x}} \times \mathbf{B} \tag{12}$$

$$\mathbf{z} = \mathbf{B} - \hat{\mathbf{x}}(\mathbf{B} \cdot \hat{\mathbf{x}}) \tag{13}$$

$$\hat{\mathbf{y}} = \frac{1}{\|\mathbf{y}\|}\mathbf{y} \tag{14}$$

$$\hat{\mathbf{z}} = \frac{1}{\|\mathbf{z}\|}\mathbf{z} \tag{15}$$

where $\mathbf{B}$ is the magnetic field vector.

From the definition of ρ [see (1)], we can then represent the incoming wave's magnetic field as

$$\mathbf{H} = \alpha(\hat{\mathbf{z}} - \rho\hat{\mathbf{y}}) \tag{16}$$

where α is an arbitrary complex number representing the amplitude and phase of the incoming wave, and ρ is the polarization defined in (9). We then assume that the response of a small loop antenna element, as described in Section II, will be proportional to the component of the $\mathbf{H}$ perpendicular to the plane of the loop.

Note that in this notation $\mathbf{H}$, which refers to the magnetic field of the incoming wave is not directly related to $\mathbf{B}$, which refers to the Earth's magnetic field.

Using the polarization results shown in Fig. 5, it is then possible to predict the response of the polarimetric antenna to ionospherically-propagated waves coming from any direction. Fig. 8 shows the results when this is done. The top row of this figure shows the results for the O mode, with the bottom row showing the X mode. The left column shows the difference in power received by each of the two loops and the right column shows the phase difference between them.

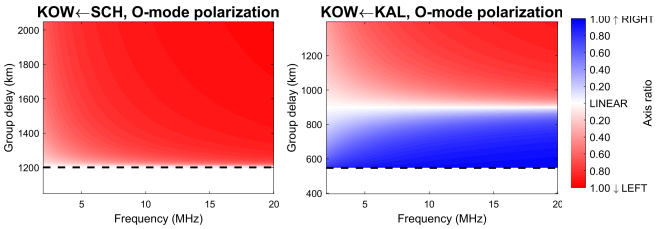

Fig. 9. Predicted O mode polarization for an OIS ionogram. Both panels are received at Kowandi. The left panel is transmitted from Scherger, the right panel is transmitted from Kalkarindji. The dashed lines on both images show the group range at which the SMM predicts an elevation of zero degrees (i.e., at the horizon); results below this group range are undefined within the model.

The most striking feature is a change in the phase difference between the two loops between the regions identified in Section III; near the horizon to the south, where $0° < \Theta < 90°$, the O mode has a phase difference of $+90°$ and the X mode has a phase difference of $-90°$, whereas in the zenith and northern directions, where $90° < \Theta < 180°$, the two modes have the opposite phases.

By combining the direction of the arrival model from Section IV, the polarization model, and (16), it is possible to predict the response of the vector antenna system to an OIS signal. Fig. 9 shows the predicted polarization of each possible pixel in an OIS ionogram, for two different paths. The left panel shows the results for Kowandi receiving Scherger. Here, the O mode is predicted to be almost perfectly circular, with a left-handed rotation, for the entire ionogram. There is only a small change in polarization at shorter group delays (thus lower elevations) and low frequencies. The right panel shows another path, Kowandi receiving Kalkarindji. Here, the geometry is such that a range of different polarizations is expected: at shorter group delays, the O mode is right-circularly polarized, at longer group delays it is left-circularly polarized, and at approximately 900 km the radio waves are expected to leave the ionosphere at right angles to the magnetic field, thus the incoming O mode is expected to be linearly polarized.

Note that in both these images, the horizontal dashed line shows the group range at which the SMM predicts an elevation of zero degrees. Below this group range, the radio waves will be blocked by the surface of the earth, thus the model does not show any results.

Figs. 10 and 11 show the predicted response of the vector antenna system to a transmitted OIS signal, for the two paths shown in Fig. 9. The most notable feature is the change in phase at a group delay of approximately 900 km on the Kowandi receiving Kalkarindji path; this is the group delay at which signals are propagating perpendicular to the magnetic field, so there is a change of polarization. Another feature is seen on both paths at lower group delays (and thus low elevations) where the separation in phase differences between the two modes becomes small due to the geometry of the antenna, as previously shown by Harris *et al.* [6].

VI. Observations

Figs. 12 and 13 show the results of an actual OIS ionogram received with the polarimetric antenna at Kowandi, transmitted

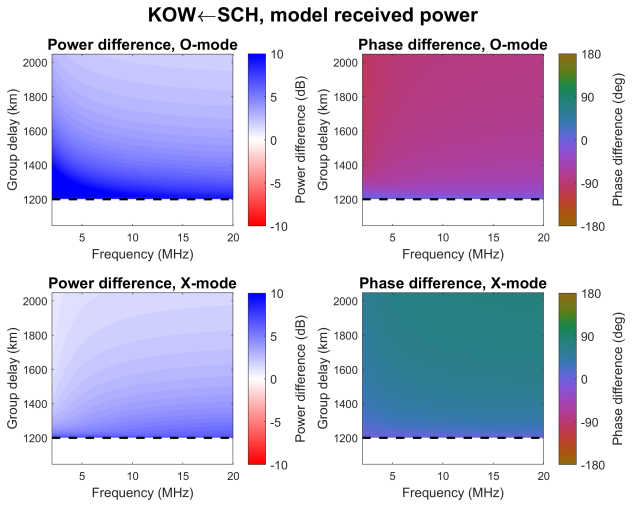

Fig. 10. Predicted response of the polarimetric antenna to an OIS ionogram received at Kowandi and transmitted from Scherger.

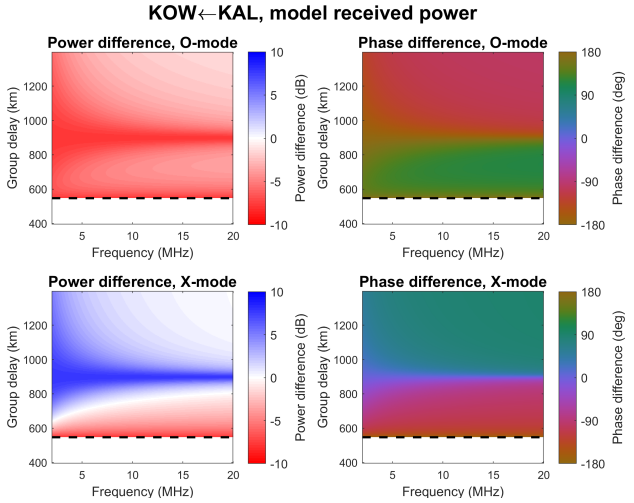

Fig. 11. Predicted response of the polarimetric antenna to an OIS ionogram received at Kowandi and transmitted from Kalkarindji.

from Scherger. This ionogram was received in June 2020 (southern hemisphere winter) during the daytime. Fig. 12 shows the power received by each of the two loops, after processing using an autoregressive interpolation technique to remove radio frequency interference [23].

Fig. 13 shows the phase differences between the two loops. The left panel shows the difference for each pixel of the ionogram. Pixels with a signal-to-noise ratio below 5 dB are not shown. For the higher delay regions of the ionogram (above 1400 km) the separation in phase difference between the O and X modes on the ionogram is clear. The right panel shows a histogram calculated for each group delay bin. Overlaid on the histogram is the estimated mean of each of the two modes for each group delay, calculated using a k-means clustering algorithm (with $k = 2$) [24]; the clusters were assigned to O and X modes according to the mean frequency of the pixels in each cluster (higher mean frequency is assigned to the X mode). Red circles indicate the mean phase difference of

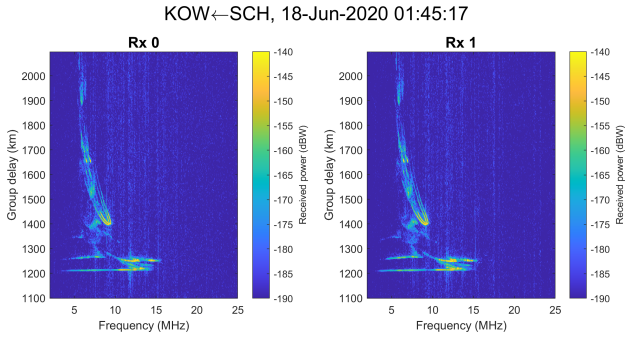

Fig. 12. Received power for each loop, for an OIS ionogram received at Kowandi and transmitted from Scherger.

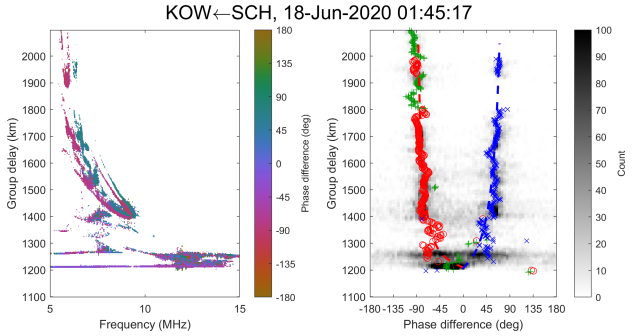

Fig. 13. Phase difference measured between the loops of the polarimetric antenna, for an OIS ionogram received at Kowandi and transmitted from Scherger. Left panel: phase difference for each pixel in the ionogram. Right panel: Histogram of phase differences, for each group delay bin. Overlaid is the estimated phase for the modes at each group delay, with the red circles for O mode, blue crosses for X mode, and green pluses for when only a single mode was present at that group delay. The dashed lines are the phase differences for the O (red) and X modes (blue) predicted by the model.

the O mode and blue crosses indicate the X mode. The green pluses indicate group delays where only one of the modes was present, i.e., the distribution of phase differences was not bimodal.

Also overlaid on the right panel in dashed lines is the phase difference predicted by the model, as shown in the right panels of Fig. 10 (specifically, the predicted difference at 6.5 MHz is shown, noting that the predictions do not have a strong frequency dependence). It can be seen that the model gives predictions that generally agree with the observations at the higher delay portions of the ionogram (above 1400 km), although for the lower portion the results are complicated by two factors.

1) The two modes will have a smaller separation in phase difference due to the geometry of the antenna [6].
2) The two modes have very close group delays and thus interfere, meaning most of the pixels cannot be cleanly separated into the two clusters. It may be possible to use signal processing techniques such as multiple signal classification (MUSIC) [25] to separate the modes; we have not yet explored this approach.

Fig. 14 shows the phase differences observed for other OISs on this same path. The agreement between the observations

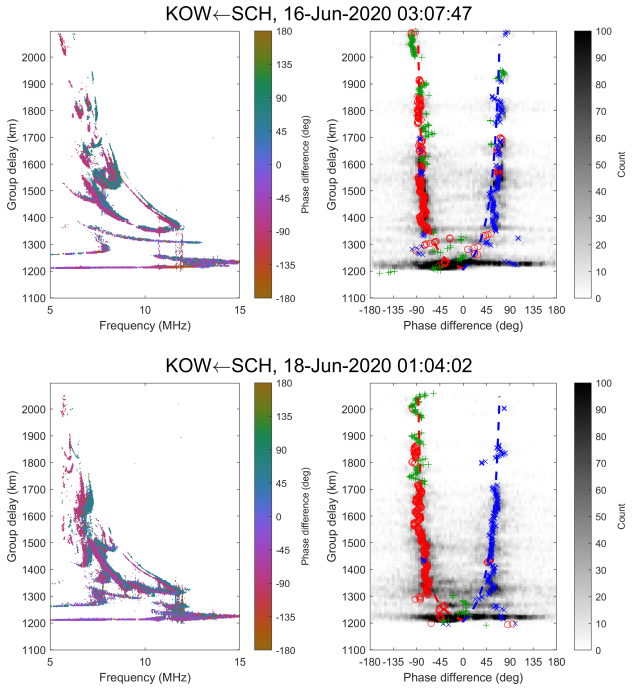

Fig. 14. Phase difference measured between the loops of the polarimetric antenna, for other OIS ionograms received at Kowandi and transmitted from Scherger. Left panels: phase difference for each pixel in the ionogram. Right panels: Histogram of phase differences, for each group delay bin, with the estimated phase for each of the modes and the model predictions overlaid similar to the right panel of Fig. 13.

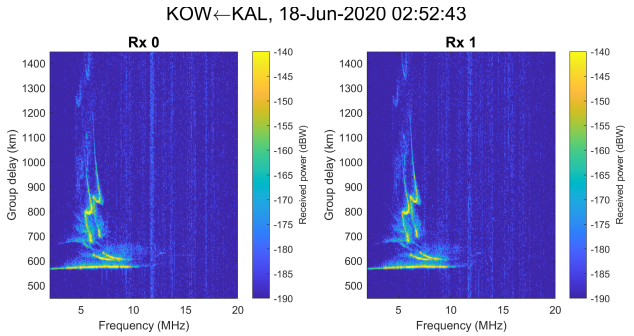

Fig. 15. Received power for each loop, for an OIS ionogram received at Kowandi and transmitted from Kalkarindji.

and the model was quite consistent across all the ionograms observed on this path.

Figs. 15 and 16 show the results of another OIS ionogram received at Kowandi, this time transmitted from Kalkarindji. Here, the effect of the change in polarization of the two modes can be observed. Fig. 16 shows the phase differences between the two loops, in a similar manner to Fig. 13. A gradient in the phase difference with respect to group delay can be seen, particularly between 800 and 1100 km in group delay. This gradient matches the predictions of the model, as shown in the right panel.

Fig. 17 shows the phase differences observed for a series of ionograms, where the F2 region of the ionogram (above approximately 900 km in group delay) shows motion in the cusp which has been associated with

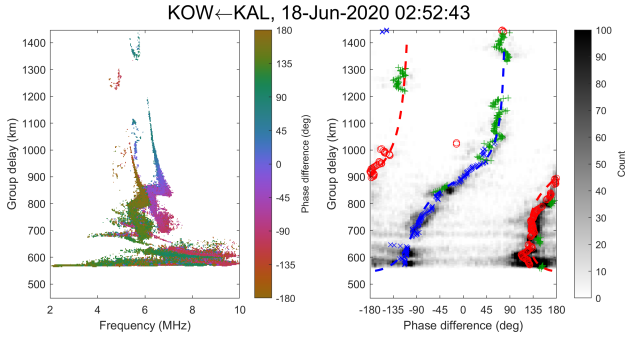

Fig. 16. Phase difference measured between the loops of the polarimetric antenna, for an OIS ionogram received at Kowandi and transmitted from Kalkarindji. Left panel: phase difference for each pixel in the ionogram. Right panel: Histogram of phase differences, for each group delay bin, with the estimated phase for each of the modes and the model predictions overlaid similar to the right panel of Fig. 13.

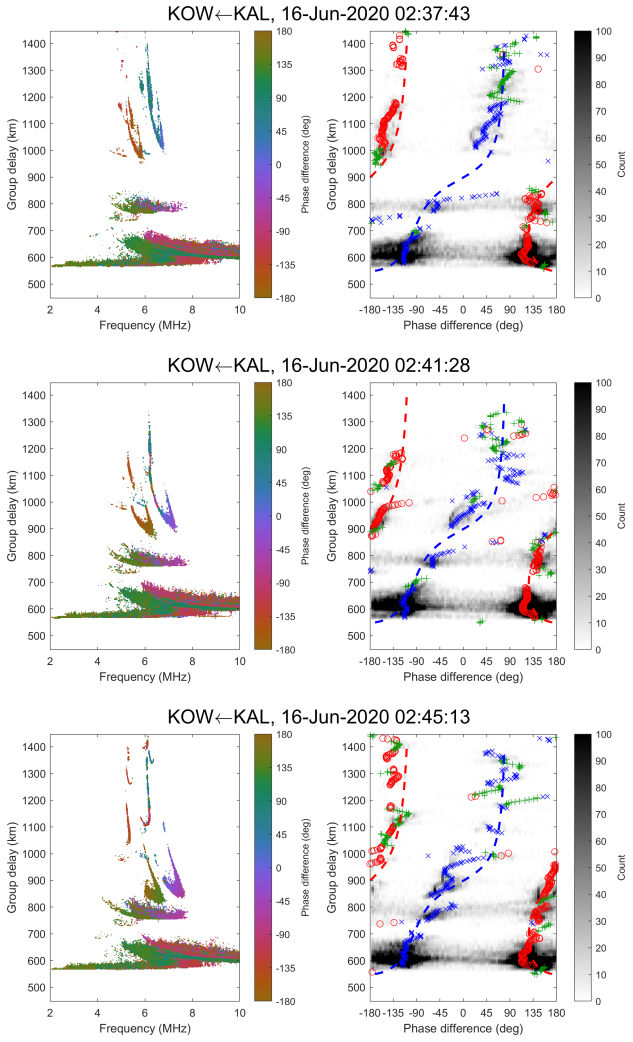

Fig. 17. Phase difference measured between the loops of the polarimetric antenna, for a series OIS ionogram received at Kowandi and transmitted from Kalkarindji, showing the passage of what appears to be a medium-scale TID. Left panels: phase difference for each pixel in the ionogram. Right panels: histogram of phase differences, for each group delay bin, with the estimated phase for each of the modes and the model predictions overlaid similar to the right panel of Fig. 13.

medium-scale TIDs [14], [26]. In this region, the observed phase differences deviate from the model predictions; this is

expected as the presence of medium-scale TIDs violates the assumptions of the SMM and will cause the incoming direction of arrival to deviate from the model's predictions.

VII. Conclusion

We have developed a model for the polarization of ionospherically propagated radio waves and validated it against real data; most notably, the polarization is dependent only upon the strength and direction of the magnetic field at the location where the radio wave exits the ionosphere and is not dependent upon the wave's path through the ionosphere. This leads to the hemisphere of possible incoming directions of arrival to any particular receiver is divided into three regions.

1) For signals received from the south, where $0° < \Theta < 90°$, the O mode is right elliptically polarized and the X mode is left elliptically polarized.
2) For signals received from the north, where $90° < \Theta < 180°$, the O mode is left elliptically polarized and the X mode is right elliptically polarized.
3) For signals received in the region where $\Theta \approx 90°$, both modes will be linearly polarized.

This model, combined with an SMM of the ionosphere, can be used to predict the polarization of a signal received from any particular transmitter as a function of the group delay of that signal. We have used this to predict the response of a polarimetric antenna to an OIS ionogram, and have shown that the model can accurately predict the phase differences observed on actual ionograms.

The birefringence of the ionosphere affects any system using ionospherically propagated radio waves, such as long-distance broadcasting, HF skywave communications, and over-the-horizon radar. This model will be useful when predicting the effectiveness of any such system.

References

[1] K. G. Budden, *The Propag. Radio Waves: The Theory Radio Waves Low Power Ionosphere Magnetosphere*. Cambridge, U.K.: Cambridge Univ. Press, 1985.

[2] I. A. Galkin, G. M. Khmyrov, A. V. Kozlov, B. W. Reinisch, X. Huang, and V. V. Paznukhov, "The ARTIST 5," in *Proc. AIP Conf.*, vol. 974, no. 1, 2008, pp. 150–159.

[3] T. J. Harris and L. H. Pederick, "A robust automatic ionospheric O/X mode separation technique for vertical incidence sounders," *Radio Sci.*, vol. 52, no. 12, pp. 1534–1543, Dec. 2017.

[4] B. W. Reinisch and H. Xueqin, "Automatic calculation of electron density profiles from digital ionograms: 3. Processing of bottomside ionograms," *Radio Sci.*, vol. 18, no. 3, pp. 477–492, May 1983.

[5] N. A. Zabotin, J. W. Wright, and G. A. Zhbankov, "NeXtYZ: Three-dimensional electron density inversion for dynasonde ionograms," *Radio Sci.*, vol. 41, no. 6, Dec. 2006.

[6] T. J. Harris, M. A. Cervera, L. H. Pederick, and A. D. Quinn, "Separation of O/X polarization modes on oblique ionospheric soundings," *Radio Sci.*, vol. 52, no. 12, pp. 1522–1533, Dec. 2017.

[7] T. J. Harris, A. D. Quinn, and L. H. Pederick, "The DST group ionospheric sounder replacement for JORN," *Radio Sci.*, vol. 51, no. 6, pp. 563–572, Jun. 2016.

[8] L. H. Pederick and M. A. Cervera, "Semiempirical model for ionospheric absorption based on the NRLMSISE-00 atmospheric model," *Radio Sci.*, vol. 49, no. 2, pp. 81–93, Feb. 2014.

[9] K. G. Budden and J. A. Ratcliffe, "The theory of the limiting polarization of radio waves reflected from the ionosphere," *Proc. Roy. Soc. London A, Math. Phys. Sci.*, vol. 215, no. 1121, pp. 215–233, 1952.

[10] M. G. W. Hayes and K. G. Budden, "Theory of the limiting polarization of radio waves emerging obliquely from the ionosphere," *Proc. Roy. Soc. London A, Math. Phys. Sci.*, vol. 324, no. 1558, pp. 369–390, 1971.

[11] E. Thébault *et al.*, "International geomagnetic reference field: The 12th generation," *Earth, Planets Space*, vol. 67, no. 1, p. 79, 2015.

[12] K. Davies, *Ionospheric Radio*. Edison, NJ, USA: IET, 1990.

[13] D. Martyn, R. Cherry, and A. Green, "Long-distance observations of radio waves of medium frequencies," *Proc. Phys. Soc.*, vol. 47, no. 2, p. 340, 1935.

[14] M. A. Cervera and T. J. Harris, "Modeling ionospheric disturbance features in quasi-vertically incident ionograms using 3-D magnetoionic ray tracing and atmospheric gravity waves," *J. Geophys. Res. Space Phys.*, vol. 119, no. 1, pp. 431–440, Jan. 2014.

[15] A. J. Heitmann *et al.*, "Observations and modeling of traveling ionospheric disturbance signatures from an australian network of oblique angle-of-arrival sounders," *Radio Sci.*, vol. 53, no. 9, pp. 1089–1107, 2018.

[16] G. G. Vertogradov, V. P. Uryadov, M. S. Sklyarevsky, and V. A. Valov, "Oblique sounding of the ionosphere by means of an ionosonde–direction finder with chirp signal," *Radiophys. Quantum Electron.*, vol. 59, no. 11, pp. 888–899, Apr. 2017.

[17] E. V. Appleton, "Two anomalies in the ionosphere," *Nature*, vol. 157, no. 3995, p. 691, 1946.

[18] D. N. Anderson, "A theoretical study of the ionospheric F region equatorial anomaly—I. Theory," *Planet. Space Sci.*, vol. 21, no. 3, pp. 409–419, Mar. 1973.

[19] D. N. Anderson, "A theoretical study of the ionospheric F region equatorial anomaly—II. Results in the American and asian sectors," *Planet. Space Sci.*, vol. 21, no. 3, pp. 421–442, Mar. 1973.

[20] R. T. Tsunoda *et al.*, "Off-great-circle paths in transequatorial propagation: 1. Discrete and diffuse types," *J. Geophys. Res. Space Phys.*, vol. 121, no. 11, pp. 11157–11175, 2016.

[21] R. T. Tsunoda *et al.*, "Off-great-circle paths in transequatorial propagation: 2. Nonmagnetic-field-aligned reflections," *J. Geophys. Res. Space Phys.*, vol. 121, no. 11, pp. 11176–11190, 2016.

[22] D. S. Kotova, M. V. Klimenko, V. V. Klimenko, and V. E. Zakharov, "Influence of geomagnetic storms of september 26–30, 2011, on the ionosphere and HF radiowave propagation. II. Radiowave propagation," *Geomagnetism Aeronomy*, vol. 57, no. 3, pp. 288–300, May 2017.

[23] M. D. E. Turley, A. J. Heitmann, and R. S. Gardiner-Garden, "Ionogram RFI rejection using an autoregressive interpolation process," *Radio Sci.*, vol. 54, no. 1, pp. 135–150, Jan. 2019.

[24] D. Arthur and S. Vassilvitskii, "k-means++: The advantages of careful seeding," Stanford InfoLab, Stanford, CA, USA, Tech. Rep., 2006. [Online]. Available: http://ilpubs.stanford.edu:8090/778/

[25] R. Schmidt, "Multiple emitter location and signal parameter estimation," *IEEE Trans. Antennas Propag.*, vol. AP-34, no. 3, pp. 276–280, Mar. 1986.

[26] T. J. Harris, M. A. Cervera, and D. H. Meehan, "SpICE: A program to study small-scale disturbances in the ionosphere," *J. Geophys. Res. Space Phys.*, vol. 117, no. A6, Jun. 2012.

Lenard Pederick received the B.Eng. degree in electrical and electronic engineering and B.Sc. (Hons.) degree in physics from the University of Adelaide, Adelaide, SA, Australia, in 2010 and 2011, respectively, where he is currently pursuing the Ph.D. degree.

Since 2011, he has been with the Defence Science and Technology Group, Australia's Department of Defence, Edinburgh, SA, working on research topics including ionospheric propagation, ionospheric sounder systems, and coordinate registration for over-the-horizon radar.

Trevor Harris received the Ph.D. degree in atmospheric physics from the University of Adelaide, Adelaide, SA, Australia, in 1993.

He has three solar cycles (more than 33 years) of experience in remote sensing, experimentation, modeling and data, signal, and image analysis of the upper atmosphere and near-space environment. He joined Australia's Department of Defence, in 1987 in the High Frequency Radar Branch of Radar Division, Defence Science and Technology Organisation, Edinburgh, SA. During this time, he has worked on spread Doppler clutter, HF communications, regional engagement, and international collaborations, and has been deeply involved in over-the-horizon radar coordinate registration research (registering radar-space measurements to ground), ionospheric specification, and the production of the operational near-real-time regional ionospheric model currently used in the Jindalee Operational Radar Network (JORN), and its improvements through JORN Phase 3 to Phase 6. His research work over the last ten years has concentrated on observation and modeling of ionospheric dynamics over varying time and spatial scales focusing on disturbances and asymmetries in the ionosphere. He left the Department of Defence and the Australian Public Service in October 2020 after a commendable 33 years of service. Since 2016, he has been an Adjunct Associate Professor with the Physics Department, School of Physical Sciences, University of Adelaide, and continues to work and research in ionospheric physics topics.

Dr. Harris was a recipient of the HJ Priestley Memorial Medal in 1984, University Medal in 1986, and various Department of Defence commendations and medals for work with over-the-horizon radar. He is the current Co-Chair of the Australian Institute of Physics National Committee on Solar-Terrestrial and Space Physics.

Andrew MacKinnon received the Ph.D. degree in physics from the University of Adelaide, Adelaide, SA, Australia, in 2001.

After his Ph.D. degree, he worked as a Post-Doctoral Fellow with the University of Adelaide. He then took up a position of a Research Scientist at Atmospheric Radar Systems, in 2003. In 2004, he returned to the University of Adelaide, becoming a Senior Research Associate, in 2008. In 2009, he accepted a position as a Lecturer and became the Inaugural First Year Director of Physics, in 2011. In 2016, he was one of the Inaugural Members of University of Adelaide Education Academy, Adelaide, SA. Since 2019, he has been the Head of the Physics Department, University of Adelaide.

Dr. MacKinnon is a member of the Australian Institute of Physics. He was on the South Australian committee from 2015 to 2020, and the Chair from 2017 to 2018. Despite being an education-focussed specialist, he has maintained his research interest by being an active member of the Space and Atmospheric Physics group at the University of Adelaide, supervising postgraduate students.

Iain Reid (Senior Member, IEEE) received the Ph.D. degree in physics and the Doctor of Science degree from the University of Adelaide, Adelaide, SA, Australia, in 1984 and 2008, respectively.

He has more than four decades of experience in remote sensing of the atmosphere and near-space environment using both radar and passive and active optical techniques. He was a Post-Doctoral Fellow with the Institute for Space and Atmospheric Science, University of Saskatchewan, Saskatoon, SK, Canada, from 1984 to 1985, and a Wissenschaftlicher Mitarbeiter with the Max Planck Institute for Aeronomy, Katlenburg-Lindau, Germany, until the end of 1988. He then took up a position in physics with the University of Adelaide. Previously, he was the Executive Dean of the University's Roseworthy Campus, Roseworthy, SA, and the Deputy Director of the Adelaide Radar Research Centre, Adelaide, SA. Prior to this, he was the Dean of Postgraduate Coursework and the Academic Director for the University's Singapore Campus, Singapore. He has also been the Head of a number of schools with the University of Adelaide, and a Board Member for a number of University of Adelaide related companies. He is an Emeritus Professor of physics with the School of Physical Sciences, University of Adelaide. He is the Executive Director of the ATRAD group of companies and has been a company director for more than 25 years.

Dr. Reid has been a Fellow of the Australian Institute of Physics and the Institute of Physics, London, U.K. Until recently, he was a member of the Australian Academy of Science National Committee for Space Science. He is also a member of the Australian Institute of Physics National Committee on Solar Terrestrial Physics.